BİTLİS EREN ÜNİVERSİTESİ
FEN BİLİMLERİ DERGİSİ

ISSN: 2147-3129 / e-ISSN: 2147-3188

**Article Type** : Research Article
**Received** : September 3, 2024
**Revised** : March 5, 2025
**Accepted** : March 13, 2025
**DOI** : 10.17798/bitlisfen.1543142

**Year** : 2025
**Volume** : 14
**Issue** : 2
**Pages** : 647-663

# IMPROVING BRAIN TUMOR DETECTION WITH DEEP LEARNING MODELS: A COMPARATIVE ANALYSIS USING MRI AND RO-SVM CLASSIFICATION

Cafer ASLIM [1], **Abidin ÇALIŞKAN** [2*]

[1] *Batman University, Electrical and Electronics Engineering Department, Batman, Türkiye*

[2] *Batman University, Computer Engineering Department, Batman, Türkiye*

**** Corresponding Author:*** *abidin.caliskan@batman.edu.tr*

## ABSTRACT

Brain tumors are one of the most important health problems that threaten human life. Therefore, accurate diagnosis at an early stage is vital. Magnetic resonance imaging (MRI) is one of the most effective and important methods for detecting brain tumors. It is thought that instead of disease detection using traditional methods, artificial intelligence-based computer applications can make significant contributions to experts in detecting brain tumors. Deep learning (DL) models, which are very popular in the scientific world today, are used extensively in the processing of images obtained in the field of health and in the detection of diseases. In this study, VGG-19, ResNet-101 and DenseNet-121 DS models trained on the ImageNet dataset were used to detect brain tumors with magnetic resonance (MR) images. The MR images used in the study were pre-processed and the excess images were identified and cropped to obtain high efficiency. After the image ratios were adjusted, random forest (RF) and support vector machines (SVM) classification algorithms were used. In the experimental studies, the highest accuracy values were achieved with DenseNet-121 using RF and SVM classification algorithms in detecting brain tumors with the proposed method. Results of 87.67% were obtained with SVM and 85.83% with RO.

**Keywords:** Brain Tumor, VGG-19, ResNet-101, DenseNet-121, Random Forest, Support Vector Machines.

# 1 INTRODUCTION

Brain tumors represent abnormal masses or structures formed by the uncontrolled proliferation of cells within the brain [1]. These structures are generally categorized into two main types: benign and malignant tumors. Benign brain tumors typically exhibit limited growth and do not spread to other tissues and organs, whereas malignant tumors tend to grow aggressively and may metastasize, spreading to other parts of the body [2]. Particularly, malignant tumors can affect vital brain functions, leading to severe neurological symptoms that can negatively impact patients' quality of life.

The diagnostic process for brain tumors is highly complex and challenging for healthcare professionals. This process includes both the detection and characterization of the tumor. Once detected, determining whether the tumor is benign or malignant is a critical step that directly influences treatment and follow-up strategies. For instance, benign tumors can often be surgically removed and generally do not recur, while malignant tumors may require more complex treatment methods and carry a high risk of recurrence. Therefore, accurate and timely diagnosis can have a direct impact on the patient's prognosis [3].

Today, medical imaging techniques play a crucial role in the detection and assessment of brain tumors. Particularly, MRI is one of the most commonly used methods due to its ability to visualize brain structures in high resolution and detail [4]. MRI provides essential information for planning surgical intervention and other treatment options by evaluating the size, location, and relationship of the tumor with surrounding tissues.

Early diagnosis of brain tumors is of critical importance for increasing patients' survival and quality of life. The mortality rate associated with brain tumors is quite high globally, which further underscores the importance of early diagnosis [5]. Brain tumors that are diagnosed early can be managed with appropriate treatment methods, potentially increasing patient survival.

Recent years have witnessed revolutionary advancements in medical imaging, largely driven by artificial intelligence (AI) and, in particular, DL techniques. DL leverages multi-layered neural networks to analyze extensive datasets, enabling the identification of complex structures and patterns [6]. In this context, DL-based methods have enabled the automatic analysis of brain MRI images, making it possible to detect tumors with high accuracy. These technological advancements have led to significant transformations in the diagnosis and management of brain tumors and are increasingly being integrated into clinical practice [7].

MRI is widely used as a technique for the detection and analysis of brain tumors. Imaging the brain in three different planes allows for a detailed examination of the tumor's morphological, textural, and volumetric characteristics [2], [8]. MRI is preferred due to its non-invasive nature and its ability to image soft tissues with high resolution [9]. Additionally, different MRI sequences reveal various characteristics of tumors, contributing to accurate diagnosis and treatment planning [10]. The analyzed MRI images will be used for tumor detection employing DL methods.

This study makes a significant contribution to the literature by demonstrating the impact of DL methods in medical imaging. A comparative analysis of modern DL architectures, specifically VGG-19, ResNet-101, and DenseNet-121, was conducted to detect brain tumors from MRI. The findings reveal that ResNet-101 offers a higher classification accuracy compared to other models, thus providing evidence in the literature for the model's effective application to medical datasets.

One of the most notable contributions of this work is the improvement in performance achieved by combining DL models with traditional classification methods such as SVM and Region Optimization. This combination, which resulted in more consistent and accurate outcomes, presents a novel perspective on optimizing DL models for medical images, differing from the approaches suggested by previous studies.

## 2 LITERATURE REVIEW

Numerous studies in the literature have focused on tumor detection from MR images using DL techniques. These studies often compare the performance of various methods, including the Gabor wavelet-based method, the statistical feature-based method, convolutional neural networks (CNN), and the ELM-LRF. Among these, the proposed method demonstrated a classification accuracy of 97.18% [8].

Additionally, in another study related to this dataset, tumor or cancer detection from medical images such as MR and CT was investigated, and the U-net model was utilized to improve the quality of the obtained images. At the end of the training, a similarity rate of 86% and a sensitivity of 80% were achieved [11]. A model based on the segmentation of MR images for brain tumor detection was proposed. In experimental studies, brain tumors were detected with 87% accuracy using the Markov random field method [12]. For classifying brain tumors,

the CapsNet model was used, aiming for high accuracy. Using 64 features obtained from a single convolutional layer, an accuracy rate of 86.56% was achieved [13].

Another study focused on steps such as preprocessing, segmentation, region of interest (ROI) determination, and tumor detection, achieving an 84.26% success rate on 497 MR slices from 10 patients. [14]. Jayakumari and Subha [15] utilized a 3D CNN model called VoxCNN for brain tumor classification. This model was applied to MRI data and achieved an accuracy rate of 98.2%. Due to its ability to learn three-dimensional features, the model demonstrated high performance in accurately classifying tumors.

Coşkun and Alkan [16] investigated brain tumor classification using the transfer learning method. Specifically, by using the pre-trained VGG16 model, they achieved 94.3% accuracy on MRI data. Transfer learning made it possible to achieve high performance even with less data.

Li et al. [17] developed a hybrid approach for brain tumor detection that combines CNN and RNN models. This model achieved an accuracy rate of 95.7% by learning both spatial and temporal features. This study demonstrates how combining DL models can be effective in learning more complex data structures. In a study conducted by Zhang and Zhang [18], a deep neural network (DNN) model supported by feature selection was proposed. This model achieved a 96.8% accuracy rate by filtering out irrelevant features in MRI data. Feature selection played a crucial role in enhancing the overall performance of the model. Liu et al. [19] performed brain tumor classification using a multilayer perceptron (MLP) model. In this study, conducted on MRI data, an accuracy rate of 92.5% was obtained. The use of MLP in conjunction with DL techniques proved effective in improving accuracy.

# 3 MATERIAL AND METHOD

## 3.1 Dataset

The dataset we used in this study, a dataset created by Abhranta Panigrahi and shared on Kaggle was used [20]. The dataset consists of three main folders: a folder for tumor images, a folder for non-tumor images, and a folder for test images. Figure 1 presents a sample of MR images from the dataset.

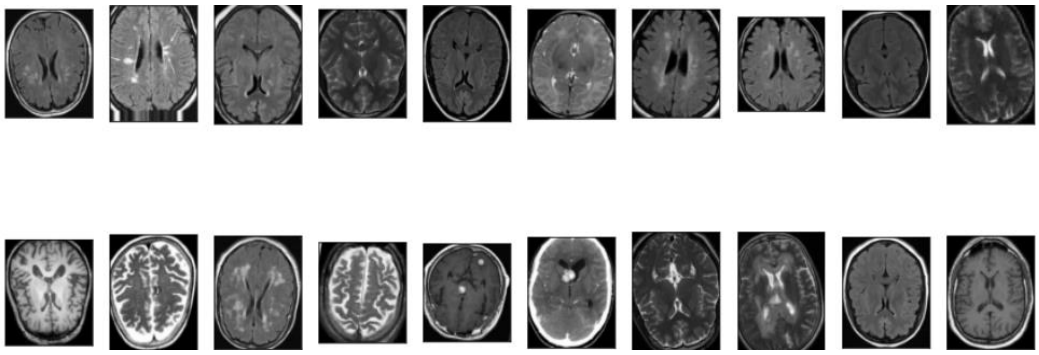

***Figure 1. Some sample images from the dataset***

A dataset consisting of 3060 MR images in total was used. The dataset was divided into three groups: The first group consisted of 1500 tumorous MR images, the second group consisted of 1500 non-tumorous MR images, and the third group consisted of 60 test images.

***Table 1. Number of Images in the Dataset***

| Image Type | Training Image |
|---|---|
| **Tumorous Images** | 1500 |
| **Non-tumorous Images** | 1500 |
| **Test Images** | 60 |

The images were standardized to obtain more efficient results from the images in the dataset (Figure 2). For this purpose, certain parts of the images were cropped using the OpenCV Library and resized to 224x224x3. The dataset was trained with ResNet-101, VGG-19 and DenseNet-121 architectures and the success rates of the models were obtained on the test images. All three architectures used are models with high success rates. In addition, the success rates of the DL models (ResNet-101, VGG-19 and DenseNet-121) were measured using RF and SVM classification algorithms on the dataset.

In the data preprocessing stage, before the tumor and non-tumor images were subjected to performance metrics, the training dataset, validation dataset, and test dataset were divided into three categories, as shown in Figure 3.

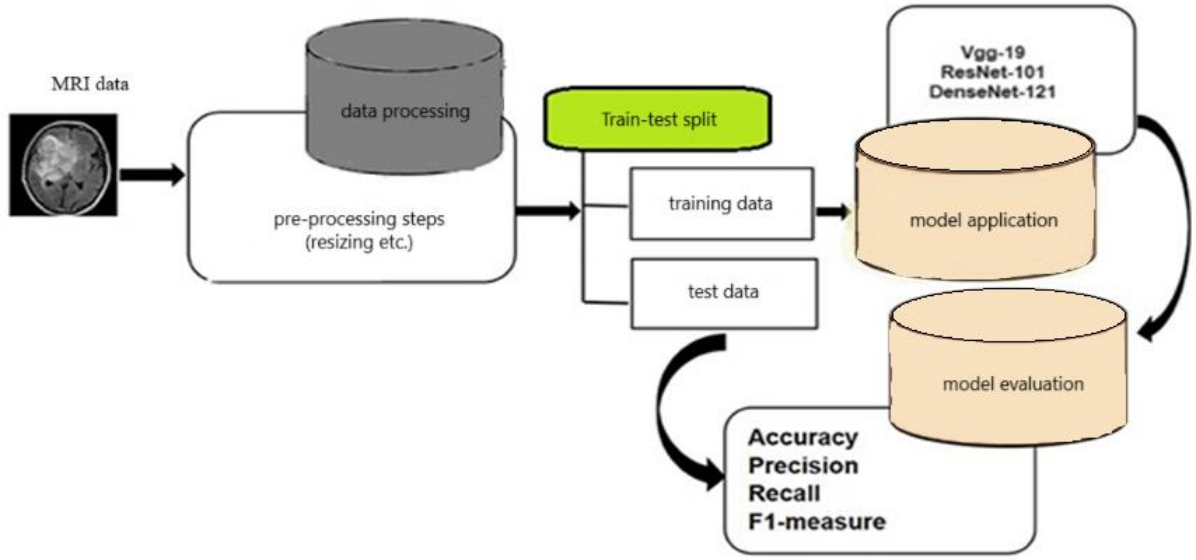


*Figure 2. Flow diagram of the study*

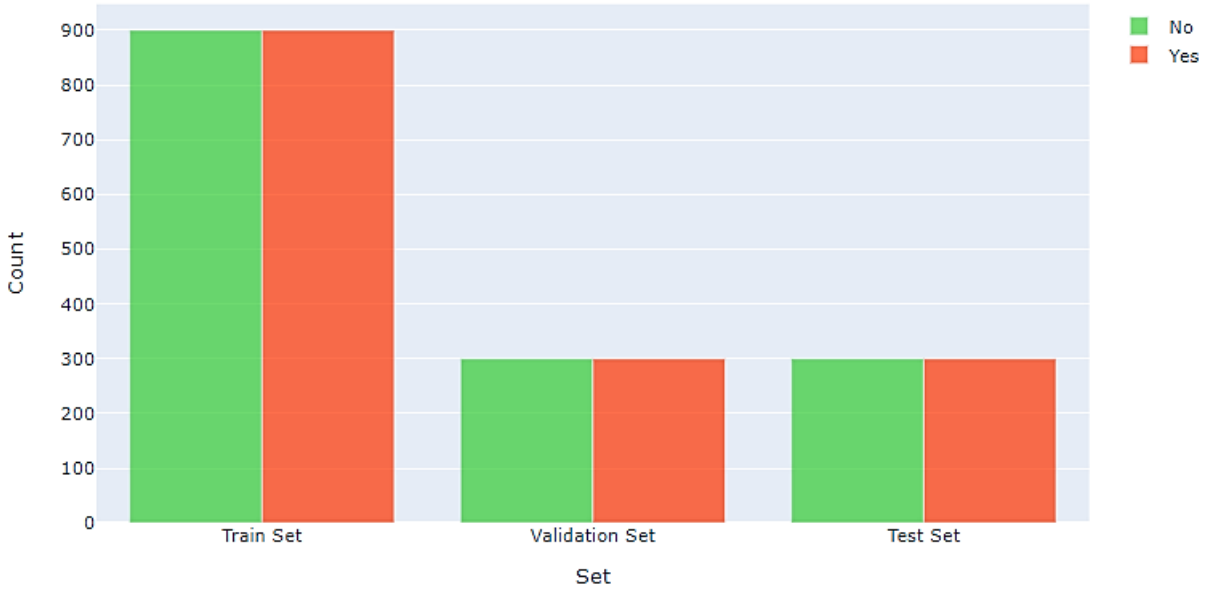


*Figure 3. Categorization of the dataset*

## 3.2 ResNet-101

ResNet architecture utilizes ResBlock layers to transfer information learned in previous layers to subsequent ones. These transfers occur via skip connections. Skip connections, situated between the weight layers and the ReLU activation function, enhance the model's learning capacity and mitigate the vanishing gradient problem. This feature offers an effective solution to the degradation issues that arise as the number of layers increases, particularly in deep neural networks (DNNs). The ResBlock structure prevents a decline in performance as the depth of the ResNet model increases, ensuring an effective learning process even in the deeper layers of the network [21].

ResNet, developed in 2015, has brought a significant innovation to the problems encountered during the training of DSA. This model won the first place in the ILSVRC (ImageNet Large Scale Visual Recognition Challenge) competition held in 2015 with a low error rate of 3.57%. ResNet-101 is a 101-layer deep neural network model and generally shows superior performance in the fields of image classification and computer vision. The success of ResNet has revealed the power of DSA models based on learning residual values and has made a great contribution to the development of this field [22].

ResNet also stands out with its ability to achieve high performance even in deep networks when compared to other architectures. This feature has enabled ResNet to be widely used in various application areas. For example, the ResNet-101 model is frequently preferred in areas requiring high accuracy such as medical image processing, autonomous vehicles and object recognition [23].

The structure of the model is shown in Figure 4. The structure of the model is shown in Figure 4.

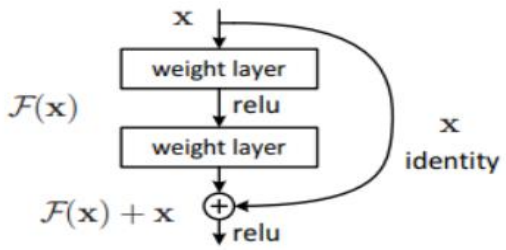


***Figure 4. ResNet-101 Structure [23]***

## 3.3 VGGNet-19

VGG-19 is a deep ESA architecture developed by the Visual Geometry Group (VGG) of Oxford University. Introduced in 2014, this model is considered one of the most successful architectures of that period and achieved great success by taking the second place in the ILSVRC 2014 competition. VGG-19's architecture has a total of 24 main layers consisting of 16 convolutional, five pooling and three fully connected layers.

This architecture optimizes the number of parameters by using small filters of 3×3 pixel size to manage the complexity of deep networks. The success of VGG-19 is important in demonstrating the power and flexibility of DL models. The model is especially useful for computing these small filter sizes, which help reduce the computational cost and increase the learning capacity of the network despite having deeper layers [24].

The success of VGG-19 is important in demonstrating the power and flexibility of DL models. The model has found a wide range of applications, especially in the fields of computer vision and image classification. Increasing the depth and number of layers allows the model to learn more complex features. However, this also means that it requires greater computational power. VGG-19 provides an optimized structure to balance these challenges. It is still used as a reference in many research and applications today [25].

One of the outstanding features of VGG-19 compared to other architectures is that the network has a regular and understandable structure despite the increased number of layers. This feature makes the model especially attractive for researchers and makes it easier to experiment on different data sets. VGG-19 is an important example that aims to establish the best balance between depth and performance in neural network architecture [26]. The VGG-19 architecture is shown in Figure 5.

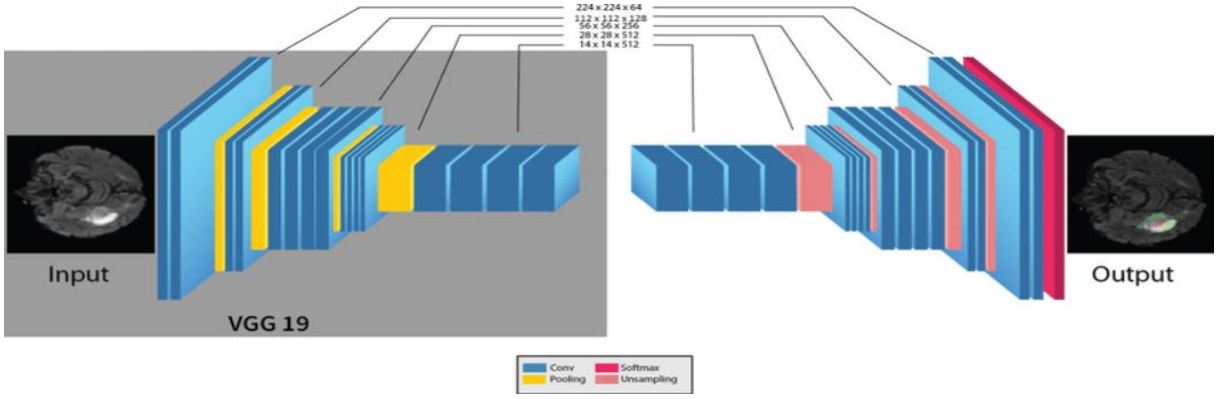


***Figure 5. VggNet-19 Architecture [27]***

## 3.4 DenseNet-121

The DenseNet model proposed by Huang et al. takes input from 224x224 images and has approximately 7 million trainable parameters. DenseNet121 can cope with the vanishing gradient problem and thus allows the construction of networks with sufficient depth, while increasing the speed of the network due to having fewer parameters than other networks [28]. The DenseNet architecture aims to solve the speed problem by densely connecting all layers.

Each new layer receives input from all previous layers and transmits its information to all subsequent layers. As a result, the last output layer receives information directly from each layer, including the first layer. In this way, it is aimed to remove unnecessary layers. In particular, the model uses skip connections to directly transmit information to different levels of dense blocks and achieve better accuracy [29].

DenseNet has shown great success in various fields, especially in applications that require processing complex data structures such as medical and biomedical image analysis. With its dense connection structure, this model allows medical images to be analyzed in more detail and accurately, which significantly increases diagnostic accuracy. One of the most striking features of DenseNet is its high performance even when working with limited data sets. This feature makes it advantageous compared to other DL models and allows it to be used in a wide range of applications from medical imaging to object recognition [30].

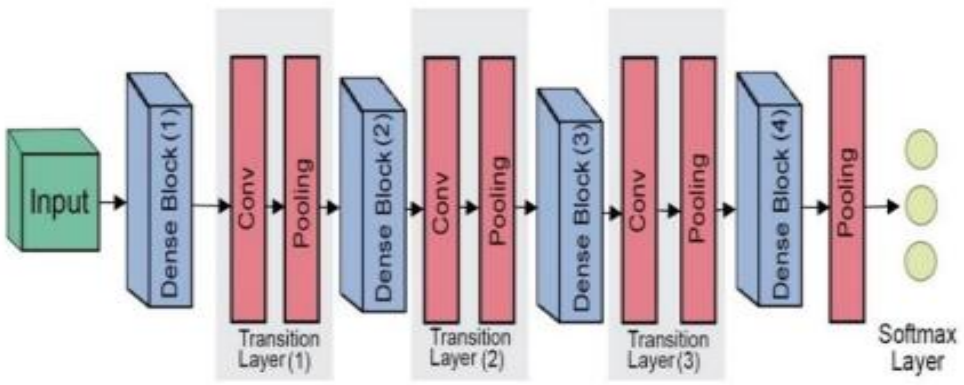


***Figure 6. DenseNet-121 architecture consisting of four dense block layers and three transition layers [31]***

## 3.5 Deep Learning Performance Metrics

Model performance metrics are used to assess the results of models employed in DL. The most common metrics for evaluating a model's performance include accuracy, precision, recall, and F1 score [32], [33], [34].

The mathematical formulas for these metrics are provided in the equations (1), (2), (3), and (4), respectively.

$$Accuracy = \frac{TP + TN}{TP + TN + TN + FN} \tag{1}$$

$$Precision = \frac{TP}{TP + FP} \tag{2}$$

$$Recall\ (Sensitivity) = \frac{TP}{TP + FN} \tag{3}$$

$$F1\ Score = 2 * \frac{Recall * Precision}{Recall + Precision} \tag{4}$$

# 4 RESULTS AND DISCUSSION

This study utilized the VGG-19, ResNet-101, and DenseNet-121 DL models, trained on the ImageNet dataset, for brain tumor detection. The models were combined with the RO and SVM classification algorithms to achieve more consistent results.

Figure 7 shows the confusion matrix for each model using RO classification. In the confusion matrix of VGG-19, out of 300 non-tumor (healthy) data points, 246 were correctly classified as non-tumor (TP), while 54 were incorrectly classified as tumor (FN). In the subsequent row, out of 300 tumor data points, 247 were correctly classified as tumor (TN), and 53 were incorrectly classified as non-tumor (FP).

Within the ResNet-101 confusion matrix, 262 out of 300 non-tumor (healthy) data points were correctly classified as non-tumor (TP), while 38 were incorrectly classified as tumor (FN). In the subsequent row, 256 out of 300 tumor data points were correctly classified as tumor (TN), and 44 were incorrectly classified as non-tumor (FP).

The confusion matrix of DenseNet-121 reveals that 267 out of 300 non-tumor (healthy) data points were correctly classified as non-tumor (TP), with 33 incorrectly classified as tumor (FN). The next row shows that 211 out of 300 tumor data points were correctly classified as tumor (TN), while 89 were incorrectly classified as non-tumor (FP)."

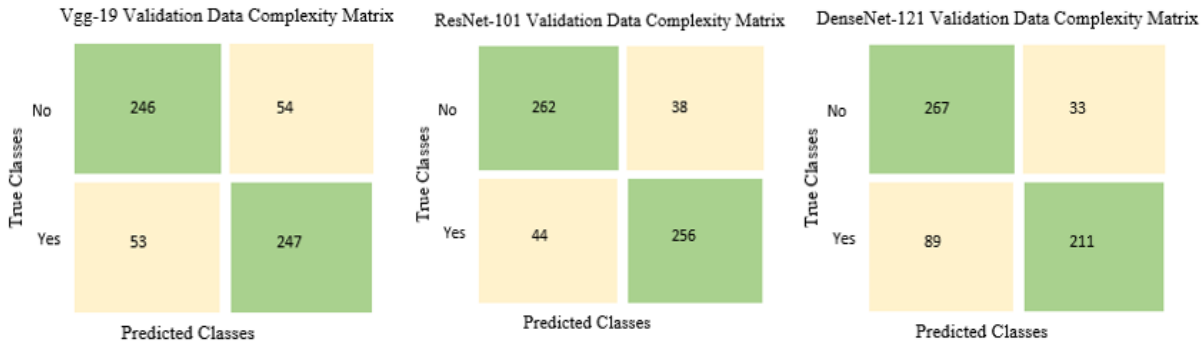


***Figure 7. Validation data of the models and RO and complexity matrix results***

For another classification algorithm, SVM, the confusion matrices are presented in Figure 8, respectively. In the confusion matrix of VGG-19, out of 300 non-tumor (healthy) data points, 241 were correctly classified as non-tumor (TP), while 59 were incorrectly classified as tumor (FN). In the subsequent row, out of 300 tumor data points, 220 were correctly classified as tumor (TN), and 80 were incorrectly classified as non-tumor (FP).

The confusion matrix of ResNet-101, out of 300 non-tumor (healthy) data points, 268 were correctly classified as non-tumor (TP), while 32 were incorrectly classified as tumor (FN). In the subsequent row, out of 300 tumor data points, 257 were correctly classified as tumor (TN), and 43 were incorrectly classified as non-tumor (FP).

In the confusion matrix of DenseNet-121, out of 300 non-tumor (healthy) data points, 241 were correctly classified as non-tumor (TP), while 59 were incorrectly classified as tumor (FN). In the subsequent row, out of 300 tumor data points, 220 were correctly classified as tumor (TN), and 80 were incorrectly classified as non-tumor (FP).

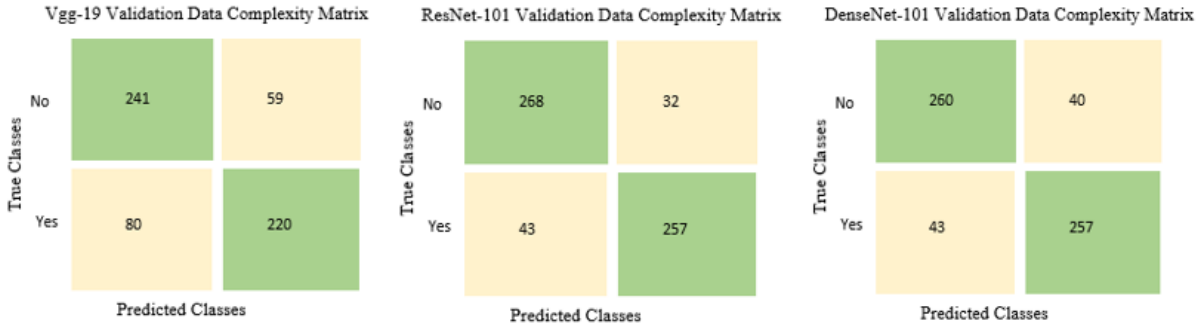


***Figure 8. Complexity matrix results of validation data of models with SVM***

The classification results on the dataset using RO and SVM classification algorithms are presented in the Tables. Such a study allows for a comparative analysis of the performance of different classifiers.

***Table 2. RO classification test data performance results***

| Model | Accuracy | F1 Score | Reliability | Sensitivity | Precision | Roc Curve |
|---|---|---|---|---|---|---|
| **Vgg-19** | %81 | 0.81 | 0.62 | 0.81 | 0.81 | 0.80 |
| **ResNet101** | %84.83 | 0.85 | 0.70 | 0.85 | 0.86 | 0.84 |
| **DenseNet121** | %79 | 0.79 | 0.58 | 0.79 | 0.8 | 0.79 |

***Table 3. Classification results with VGG-19 RO***

| | Precision | Sensitivity | F1 Score | Sample Size |
|---|---|---|---|---|
| **Non-tumorous** | 0.82 | 0.80 | 0.81 | 300 |
| **Tumorous** | 0.80 | 0.82 | 0.81 | 300 |
| **Accuracy** | | | 0.81 | 600 |
| **Overall Avg.** | 0.81 | 0.81 | 0.81 | 600 |
| **Weighted Avg.** | 0.81 | 0.81 | 0.81 | 600 |

*Table 4. Classification results with ResNet-101 RO*

| | Precision | Sensitivity | F1 Score | Sample Size |
|---|---|---|---|---|
| Non-tumorous | 0.86 | 0.86 | 0.86 | 300 |
| Tumorous | 0.86 | 0.86 | 0.86 | 300 |
| Accuracy | | | 0.86 | 600 |
| Overall Avg. | 0.86 | 0.86 | 0.86 | 600 |
| Weighted Avg. | 0.86 | 0.86 | 0.86 | 600 |

*Table 5. Classification results with DenseNet-121 RO*

| | Precision | Sensitivity | F1 Score | Sample Size |
|---|---|---|---|---|
| **Non-tumorous** | 0.82 | 0.80 | 0.81 | 300 |
| **Tumorous** | 0.81 | 0.83 | 0.82 | 300 |
| **Accuracy** | | | 0.81 | 600 |
| **Overall Avg.** | 0.81 | 0.81 | 0.81 | 600 |
| **Weighted Avg.** | 0.81 | 0.81 | 0.81 | 600 |

*Table 6. Test data performance results with SVM classification*

| Model | Accuracy | F1 Score | Reliability | Sensitivity | Precision | Roc Curve |
|---|---|---|---|---|---|---|
| **Vgg-19** | %75.67 | 0.76 | 0.51 | 0.76 | 0.76 | 0.75 |
| **ResNet101** | %87.67 | 0.88 | 0.75 | 0.88 | 0.88 | 0.87 |
| **DenseNet121** | %75.67 | 0.76 | 0.51 | 0.76 | 0.76 | 0.75 |

*Table 7. Classification results with VGG19 and SVM*

| | Precision | Sensitivity | F1 Score | Sample Size |
|---|---|---|---|---|
| **Non-tumorous** | 0.74 | 0.80 | 0.77 | 300 |
| **Tumorous** | 0.78 | 0.72 | 0.75 | 300 |
| **Accuracy** | | | 0.76 | 600 |
| **Overall Avg.** | 0.76 | 0.76 | 0.76 | 600 |
| **Weighted Avg.** | 0.76 | 0.76 | 0.76 | 600 |

*Table 8. Classification results with ResNet-101 and SVM*

| | Precision | Sensitivity | F1 Score | Sample Size |
|---|---|---|---|---|
| **Non-tumorous** | 0.87 | 0.89 | 0.88 | 300 |
| **Tumorous** | 0.88 | 0.87 | 0.88 | 300 |
| **Accuracy** | | | 0.88 | 600 |
| **Overall Avg.** | 0.88 | 0.88 | 0.88 | 600 |
| **Weighted Avg.** | 0.88 | 0.88 | 0.88 | 600 |

*Table 9. Classification results with DenseNet-121 and SVM*

| | Precision | Sensitivity | F1 Score | Sample Size |
|---|---|---|---|---|
| **Non-tumorous** | 0.74 | 0.80 | 0.77 | 300 |
| **Tumorous** | 0.78 | 0.72 | 0.75 | 300 |
| **Accuracy** | | | 0.76 | 600 |
| **Overall Avg.** | 0.76 | 0.76 | 0.76 | 600 |
| **Weighted Avg.** | 0.76 | 0.76 | 0.76 | 600 |

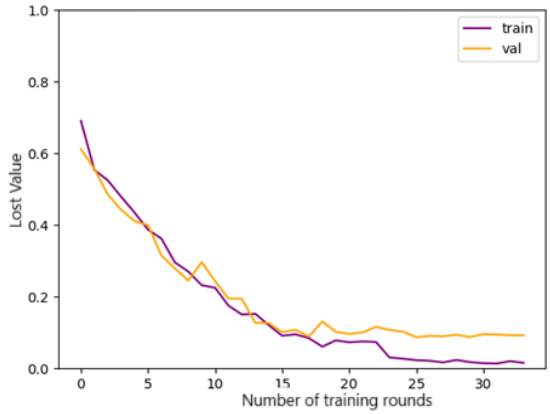


*Figure 9. Validation value of dataset*

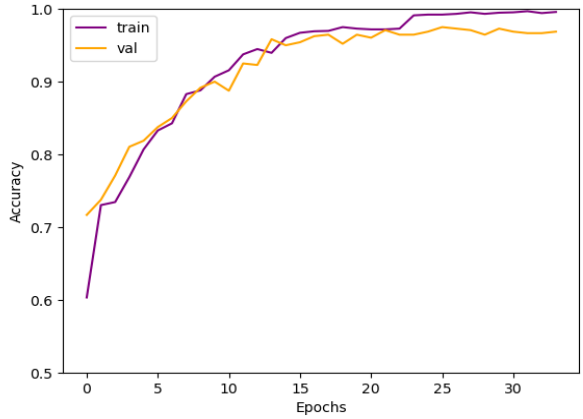


*Figure 10. Lost value of the dataset*

## 5 CONCLUSION AND SUGGESTIONS

In this study, RF and SVM with VGG-19, ResNet-101 and DenseNet-121 DL models were used to classify 3060 MR images. Complexity matrix results were obtained with various ratios on training, validation and test data. The obtained results are presented in detail below.

*Table 10. Validation Data of VGG19 with SVM and RO*

| | SVM | RO |
|---|---|---|
| **Training Set** | %82,89 | %100 |
| **Validation Set** | %76,83 | %82,17 |
| **Test Set** | %76,67 | %81,0 |

***Table 11. Validation Data with DenseNet121 SVM and RO***

| | SVM | RO |
|---|---|---|
| **Training Set** | %82 | %100 |
| **Validation Set** | %76,83 | %81,17 |
| **Test Set** | %75,67 | %81,33 |

***Table 12. Validation Data with ResNet-10 SVM and RO***

| | SVM | RO |
|---|---|---|
| **Training Set** | %92,94 | %100 |
| **Validation Set** | %87,5 | %86,33 |
| **Test Set** | %87,67 | %85,83 |

***Table 13. Accuracy rates of different studies on datasets containing MR images***

| References | Feature Extraction Method | Classification Method | Accuracy |
|---|---|---|---|
| Ahmad et al., (2022) | VGG-19 | SVM | %99,39 |
| Venmathi et al., (2023) | VGG-19 | FCM | %99,7 |
| Podder et al., (2021) | VGG-19 | | %85,32 |
| Mohsen et al., (2023) | VGG-19 | SISR | %99,89 |
| Ullah et al., (2022) | Inceptionresnetv2 | SVM | %98,91 |
| Masood et al.,2021) | ResNet-50 | Mask-RCNN | %98,34 |
| Jayakumari and Subha (2019) | 3D CNN | VoxCNN | %98,2 |
| Çoşkun and Alkan (2020) | VGG16 | CNN | %94,3 |
| Li et al., (2021) | CNN and RNN | CNN ve RNN | %95,7 |
| Zhang and Zhang (2022) | Attribute Selection | DSA | %96,8 |
| Liu et al., (2020) | Multi-Layer Perceptron | DSA | %92,5 |
| Proposed Model | **ResNet-101** | SVM | **%87,67** |

VGG-19 Model: The model demonstrated a successful performance on the training set with an accuracy rate of 82.89%. However, the validation and test sets yielded results of 76.83% and 76.67%, respectively, indicating a slight decrease in performance during the validation and testing phases. This suggests that the model may have a tendency towards overfitting during training.

DenseNet-121 Model: Similarly, this model achieved an accuracy rate of 82% on the training set. However, with accuracy rates of 76.83% on the validation set and 75.67% on the

test set, the model appears to maintain a generally balanced performance. The dense connectivity structure of DenseNet-121 may facilitate deeper learning and enhance performance, but caution should be exercised to avoid the risk of overfitting.

ResNet-101 Model: The ResNet-101 model exhibited a notably superior performance with a high accuracy rate of 92.94% on the training set, clearly outperforming the other models.

In the validation and test sets, results of 87.5% and 87.67% were obtained, respectively. This indicates that the model maintained its overall performance by minimizing the risk of overfitting to the training data.

The high accuracy of ResNet-101 can be attributed to the effectiveness of its deeper layer structure and residual blocks (ResBlocks). Overall, while the ResNet-101 model offers the highest accuracy, the VGG-19 and DenseNet-121 models also stand out with their balanced performances. When choosing between these models, it is important to consider the application domain and the characteristics of the datasets to determine which model is more suitable.

Considering all the results, it was observed that the ResNet-101 model achieved the highest correct classification rate and the lowest error values, especially on the test set. These findings suggest that among the classification algorithms used for tumor detection from MR images, the combination of DL models with SVM, particularly the ResNet-101 model, proved to be more effective. In conclusion, this study demonstrates that DL models are an effective approach for the classification of MR images, with the ResNet-101 model being particularly suitable for such applications

## Conflict of Interest Statement

There is no conflict of interest between the authors.

## Statement of Research and Publication Ethics

The study is complied with research and publication ethics.

## Artificial Intelligence (AI) Contribution Statement

This manuscript was entirely written, edited, analyzed, and prepared without the assistance of any artificial intelligence (AI) tools. All content, including text, data analysis, and figures, was solely generated by the authors.

## Contributions of the Authors

A.Ç. and C.A. designed the study, performed the experiments and wrote the article. C.A. performed the calculations, A.Ç checked the language and contributed to the writing of the manuscript.

## REFERENCES


[1] B. Özcan and H. Bakır, "Tumor Detection on Brain Images Supported by Artificial Intelligence," in *Int. Conf. On Pioneer and Innovative Studies*, 2023, vol. 1, pp. 297-306.

[2] M. Aslan, "Automatic Brain Tumor Detection Based on Deep Learning," *Fırat Univ. J. Eng. Sci.*, vol. 34, no. 1, pp. 399-407, 2022.

[3] S. A. Y. Al-Galal, I. F. T. Alshaikhli, and M. M. Abdulrazzaq, "MRI Brain Tumor Medical Images Analysis Using Deep Learning Techniques: A Systematic Review," *Health Technol.*, vol. 11, pp. 267-282, 2021.

[4] A. R. I. Ali and D. Hanbay, "Tumor Detection in MRI Images Based on Regional Convolutional Neural Networks," *Gazi Univ. J. Eng. Archit. Fac.*, vol. 34, no. 3, pp. 1395-1408, 2018.

[5] V. S. Lotlikar, N. Satpute, and A. Gupta, "Brain Tumor Detection Using Machine Learning and Deep Learning: A Review," *Curr. Med. Imaging*, vol. 18, no. 6, pp. 604-622, 2022.

[6] Y. LeCun, Y. Bengio, and G. Hinton, "Deep Learning," *Nature*, vol. 521, no. 7553, pp. 436-444, 2015.

[7] E. Yüzgeç and M. Talo, "Classification of Alzheimer's and Parkinson's Diseases Using Deep Learning Techniques," *Fırat Univ. J. Eng. Sci.*, vol. 35, no. 2, pp. 473-482, 2023.

[8] A. Ari and D. Hanbay, "Deep Learning Based Brain Tumor Classification and Detection System," *Turk. J. Electr. Eng. Comput. Sci.*, vol. 26, no. 5, pp. 2275-2286, 2018.

[9] M. Havaei et al., "Brain Tumor Segmentation with Deep Neural Networks," *Med. Image Anal.*, vol. 35, pp. 18-31, 2017.

[10] S. M. Reza and K. M. Iftekharuddin, "Multi-Fractal Texture Features for Brain Tumor and Edema Segmentation," *Biomed. Signal Process. Control*, vol. 41, pp. 39-46, 2018.

[11] A. G. Eker and N. Duru, "Applications of Deep Learning in Medical Image Processing," *Acta Infologica*, vol. 5, no. 2, pp. 459-474, 2021.

[12] F. Bulut, İ. Kılıç, and İ. F. İnce, "Comparison and Analysis of the Success of Image Segmentation Methods in Brain Tumor Detection," *Dokuz Eylül Univ. Fac. Eng. J. Sci. Eng.*, vol. 20, no. 58, pp. 173-186, 2018.

[13] P. Afshar, A. Mohammadi, and K. N. Plataniotis, "Brain Tumor Type Classification via Capsule Networks," in *Proc. 2018 25th IEEE Int. Conf. Image Process. (ICIP)*, 2018, pp. 3129-3133.

[14] S. Kazdal, B. Doğan, and A. Y. Çamurcu, "Computer-Aided Detection of Brain Tumors Using Image Processing Techniques," in *Proc. 2015 23rd Signal Process. Commun. Appl. Conf. (SIU 2015)*, pp. 863-866.

[15] J. Jayakumari and T. A. Subha, "3D CNN Model for Brain Tumor Classification Using MRI," *IEEE Access*, vol. 7, pp. 15055-15062, 2019.

[16] M. Çoşkun and A. Alkan, "Transfer Learning Based Convolutional Neural Network for Brain Tumor Classification," *Int. J. Imaging Syst. Technol.*, vol. 30, no. 1, pp. 104-112, 2020.

[17] S. Li, H. Wang, and Y. Zhang, "Hybrid CNN-RNN Model for Brain Tumor Detection," *J. Biomed. Inform.*, vol. 118, p. 103785, 2021.,

[18] X. Zhang and W. Zhang, "Feature Selection Assisted Deep Neural Networks for Brain Tumor Classification," *Comput. Biol. Med.*, vol. 144, p. 104944, 2022.

[19] Y. Liu, L. Chen, and Y. Feng, "Multilayer Perceptron Neural Network for Brain Tumor Classification," *Pattern Recognit. Lett.*, vol. 131, pp. 35-41, 2020.

[20] Kaggle, "Brain Tumor Detection MRI Dataset," Available: https://www.kaggle.com/datasets/abhranta/brain-tumor-detection-mri. Accessed: Mar. 4, 2024.

[21] A. Çalışkan, "Finding Complement of Inefficient Feature Clusters Obtained by Metaheuristic Optimization Algorithms to Detect Rock Mineral Types," *Trans. Inst. Meas. Control*, vol. 45, no. 10, pp. 1815-1828, 2023.

[22] C. Szegedy, S. Ioffe, V. Vanhoucke, and A. A. Alemi, "Inception-v4, Inception-ResNet and the Impact of Residual Connections on Learning," in *Proc. AAAI*, 2017, vol. 4, no. 1, pp. 12.

[23] B. Aksoy and O. K. M. Salman, "Prediction of Covid-19 Disease with ResNet-101 Deep Learning Architecture Using Computerized Tomography Images," *Turk. J. Nat. Sci.*, vol. 11, no. 2, pp. 36-42, 2022.

[24] M. Toğaçar, B. Ergen, and F. Özyurt, "Classification of Flower Images Using Feature Selection Methods in Convolutional Neural Network Models," *Fırat Univ. J. Eng. Sci.*, vol. 32, no. 1, pp. 47-56, 2020.

[25] K. Simonyan and A. Zisserman, "Very Deep Convolutional Networks for Large-Scale Image Recognition," *arXiv preprint arXiv: 1409.1556*, 2014.

[26] A. Çalışkan, "Classification of Tympanic Membrane Images Based on VGG16 Model," *Kocaeli J. Sci. Eng.*, vol. 5, no. 1, pp. 105-111, 2022.

[27] A. Nawaz et al., "VGG-UNET for Brain Tumor Segmentation and Ensemble Model for Survival Prediction," in *Proc. 2021 Int. Conf. Robot. Autom. Ind. (ICRAI)*, Rawalpindi, Pakistan, 2021, pp. 1-6.

[28] N. Şahin, N. Alpaslan, M. İlçin, and D. Hanbay, "Classification of Grasshopper Species, a Plant Pest, Using Convolutional Neural Network Architectures and Transfer Learning," *Fırat Univ. J. Eng. Sci.*, vol. 35, no. 1, pp. 321-33, 2023.

[29] V. Tümen, "SpiCoNET: A hybrid deep learning model to diagnose COVID-19 and pneumonia using chest X-ray images," *Traitement du Signal*, vol. 39, no. 4, pp. 1169, 2022.

[30] W. Zhu et al., "AnatomyNet: Deep Learning for Fast and Fully Automated Whole-Volume Segmentation of Head and Neck Anatomy,"*Med. Phys.*, vol. 46, no. 3, pp. 576-586, 2018.

[31] S. A. Albelwi, "Deep Architecture Based on DenseNet-121 Model for Weather Image Recognition," *Int. J. Adv. Comput. Sci. Appl.*, vol. 13, no. 10, pp. 559-565, 2022.

[32] E. Başaran, Z. Cömert and Y. Çelik, "Neighbourhood component analysis and deep feature-based diagnosis model for middle ear otoscope images," *Neural Computing and Applications*, pp. 1-12, 2022.

[33] S. B. Çelebi and Ö. A. Karaman, "Multilayer LSTM Model for Wind Power Estimation in the Scada System," *Eur. J. Tech.*, vol. 13, no. 2, pp. 116-122, 2023.

[34] G. Çelik and E. Başaran, "Proposing a new approach based on convolutional neural networks and random forest for the diagnosis of Parkinson's disease from speech signals," *Applied Acoustics*, vol. 211, p. 109476, 2023.